Probing Specificities of Alcohol Acyltransferases for Designer Ester Biosynthesis with a High-Throughput Microbial Screening Platform

Jong-Won Lee[1,2], Hyeongmin Seo[2,3], Caleb Young[3], and Cong T. Trinh[1,2,3,*]

[1]Bredesen Center for Interdisciplinary Research and Graduate Education, University of Tennessee, Knoxville, TN, USA

[2]Center for Bioenergy Innovation, Oak Ridge National Laboratory, Oak Ridge, TN, USA

[3]Department of Chemical and Biomolecular Engineering, University of Tennessee, Knoxville, TN, USA

[*]Corresponding author. Email: ctrinh@utk.edu

ABSTRACT

Alcohol acyltransferases (AATs) enables microbial biosynthesis of a large space of esters by condensing an alcohol and an acyl CoA. However, substrate promiscuity of AATs prevents microbial biosynthesis of designer esters with high selectivity. Here, we developed a high-throughput microbial screening platform that facilitates rapid identification of AATs for designer ester biosynthesis. First, we established a microplate-based culturing technique with *in situ* fermentation and extraction of esters. We validated its capability in rapid profiling of the alcohol substrate specificity of 20 chloramphenicol acetyltransferase variants derived from *Staphylococcus aureus* (CAT_{Sa}) for microbial biosynthesis of acetate esters with various exogeneous alcohol supply. By coupling the microplate-based culturing technique with a previously established colorimetric assay, we developed a high-throughput microbial screening platform for AATs. We demonstrated that this platform could not only confirm CAT_{Sa} F97W with enhanced isobutyl acetate synthesis but also identify three $ATF1_{Sc}$ (P348M, P348A, and P348S) variants, derived from *Saccharomyces cerevisiae*'s AAT and engineered by model-guided protein design, for enhanced butyl acetate production. We anticipate the high-throughput microbial screening platform is a useful tool to identify novel AATs that have important roles in nature and industrial biocatalysis for designer bioester production.

Keywords:

High-throughput microbial screening; esters; isobutyl acetate; n-butyl acetate; ethyl acetate, 2-phenhylethyl acetate; alcohol acetyltransferase; AAT; chloramphenicol acetyltransferase; CAT; *Escherichia coli;* solvent overlays; colorimetric assay; model-guided protein design.

1. INTRODUCTION

Esters are an important class of industrial chemicals with broad applications as flavors, fragrances, cosmetics, pharmaceuticals, green solvents, and advance biofuels (Lee and Trinh 2020). Currently, esters are mainly produced by chemical synthesis from petroleum-based feedstocks that are neither renewable nor sustainable (Seo et al. 2019). Alternatively, microbial conversion has emerged as an alternative route for renewable and sustainable production of esters (Layton and Trinh 2014; Layton and Trinh 2016a; Layton and Trinh 2016b; Lee and Trinh 2019; Rodriguez et al. 2014; Tai et al. 2015b). Critical to the microbial biosynthesis of esters is the requirement of alcohol acyltransferases (AATs, EC 2.3.1.84) that catalyze a thermodynamically favorable condensation of an alcohol and acyl-CoA in an aqueous environment. Since esters are commonly found in nature such as fruits (e.g., apple (Li et al. 2006; Souleyre et al. 2014; Souleyre et al. 2005), apricot (Gonzalez-Aguero et al. 2009), banana (Beekwilder et al. 2004), melon (El-Sharkawy et al. 2005; Lucchetta et al. 2007), papaya (Balbontin et al. 2010), and strawberry (Aharoni et al. 2000; Beekwilder et al. 2004; Cumplido-Laso et al. 2012; Gonzalez et al. 2009)) or yeast fermentation (Tai et al. 2015b; Verstrepen et al. 2003), various eukaryotic AATs have been identified and recently exploited for microbial biosynthesis of esters using synthetic biology and metabolic engineering approaches (Layton 2014; Lee and Trinh 2018; Rodriguez et al. 2014; Tai et al. 2015a). Recent discovery and repurposing of prokaryotic chloramphenicol acetyltransferases (CATs, EC 2.3.1.28) to function as AATs have further expanded the library of ester-producing enzymes (Rodriguez et al. 2014; Seo et al. 2019). However, due to substrate promiscuity of these AAT/CAT enzymes, controllable microbial synthesis of designer esters with high selectivity remains a significant challenge (Layton and Trinh 2014; Lee and Trinh 2019).

Bioprospecting and protein engineering are promising strategies to find novel AATs with high specificity and activity toward a target ester. For instance, AAT of *Actinidia*

chinensis (AAT_{Ac}) was engineered to create a AAT_{Ac} S99G variant that enhanced butyl octanoate production in *Escherichia coli* about 4.5-fold higher than the wildtype (Chacon et al. 2019). Similarly, Seo *at al.* reported that a single F97W mutation in CAT of the mesophilic *Staphylococcus aureus* (CAT_{Sa}), identified by a model-guided protein design, achieved ~3.5-fold increase in isobutyl acetate (IBA) production in a thermophilic, cellulolytic bacterium *Clostridium thermocellum* (Seo et al. 2019). By combining both bioprospecting and model-guided protein engineering strategies, novel CATs have recently been discovered with improved efficiency, robustness, and compatibility (Seo et al. 2020). Even though research efforts in identifying beneficial AATs/CATs with high specificity and activities are promising, large space of novel AATs/CATs are still underexplored.

To access the specificities and activities of AATs/CATs directly, the enzymes need to be purified and characterized. Two colorimetric assays have been developed to determine AAT/CAT activities including the 5,5′-dithiobis-(2-nitrobenzoic acid) (DTNB) assay (Kruis et al. 2017; Seo et al. 2019; Tai et al. 2015b) and the α-ketoglutarate dehydrogenase (α-KGDH)-coupled assay (Knight et al. 2014; Lin et al. 2016). These assays are designed to quantify free CoAs released from the AAT/CAT esterification of alcohols and acyl-CoAs by measuring either the 412 nm absorbance of yellowish 5-thio-2-nitrobenzoic acid (TNB) for the DTNB assay or the 340 nm absorbance of nicotinamide adenine dinucleotide (NADH) for (α-KGDH)-coupled assay. The key advantage of direct AAT/CAT measurement is that the assays can be performed in a high-throughput manner; however, some disadvantages for screening a large space of AATs/CATs include requirement of expensive acyl-CoA reagents and enzyme purification. Alternatively, direct measurement of esters for rapid, high-throughput screening of AAT/CAT specificities and activities *in vivo* can be attractive before determining the catalytic efficiencies in depth for promising enzyme candidates. Here, esters produced by microorganisms can be extracted with a solvent (e.g., hexane or hexadecane) and measured in

a separate step. While the conventional gas chromatography coupled with mass spectrometer (GC/MS) is accurate in identifying and quantifying esters, it is low-throughput and expensive. Fortunately, the colorimetric assay, based on the hydroxylamine/iron chemistry, can rapidly quantify esters in a high-throughput manner by first generating the ferric hydroxamate via the two steps of chemical reactions and then measuring its absorbance at 520 nm (Hill 1946; Lobs et al. 2016; Stern and Shapiro 1953; Wofford et al. 1986).

In this study, we aimed to develop a high-throughput microbial screening platform to identify novel AATs/CATs for designer ester biosynthesis in a simple, rapid, and efficient manner. We started by establishing a microplate-based culturing technique with *in situ* fermentation and extraction of esters. By coupling the microplate-based culturing technique with a modified colorimetric assay, we developed a high-throughput microbial screening platform to identify novel AATs. The platform can measure both esters and cell growth, which helps not only screen relative AATs/CATs specificities and activities rapidly but also evaluate the effect of expressing these enzymes on microbial health. We validated the developed high-throughput microbial screening platform by probing the alcohol substrate preference of 20 engineered CAT F97 variants and identifying beneficial enzyme mutants from a library of $ATF1_{Sc}$, generated by model-guided protein design, for enhanced butyl acetate production. We anticipate the high-throughput microbial screening platform is a useful tool to identify novel AATs that have important roles in nature and industrial biocatalysis for designer bioester production.

2. MATERIALS AND METHODS

2.1 Strains and plasmids. Strains and plasmids used in this study are listed in Table 1. *E. coli* TOP10 was used for molecular cloning while BL21 (DE3) or EcDL002 (Layton and Trinh 2014) was used as a host strain for ester production. The pETDuet-1 plasmids containing 20

F97 variants of CAT_{Sa} were used to examine the role of the F97 residue on the alcohol substrate preference. The plasmid $pATF1_{Sc}$ was constructed by subcloning *$ATF1_{Sc}$* gene from pDL004 (Layton and Trinh 2016a) into pET29 by the Gibson gene assembly method (Gibson et al. 2009). The $ATF1_{Sc}$ variants were generated by site-directed mutagenesis (Zheng et al. 2004). All the constructed plasmids were introduced into the host strains by chemical transformation. The primers used in this study are listed in Table S1. The alphabets annotate the amino acid variants, including: R, arginine; H, histidine; K, lysine; D, aspartic acid; E, glutamic acid; S, serine; T, threonine; N, asparagine; Q, glutamine; C, cysteine; G, glycine; Y, tyrosine; P, proline; A, alanine; V, valine; I, isoleucine; L, leucine; M, methionine; F, phenylalanine; and W, tryptophan.

2.2 Culture media. The lysogeny broth (LB) medium, comprising of 10 g/L peptone, 5 g/L yeast extract, and 5 g/L NaCl, was used for molecular cloning and seed cultures. The M9 hybrid medium (Layton and Trinh 2014) with 20 g/L glucose was used for ester production. Either 50 µg/mL ampicillin (Amp) or 50 µg/mL kanamycin (Kan) was added to the media for selection where applicable.

2.3 Microplate-based microbial screening method. Cell inoculum was prepared either from a bacterial glycerol stock or from a single colony on a LB agar plate. Specifically, 1% (v/v) of stock cells were grown overnight in 5 mL of LB at 37°C and 200 rpm on a 75° angled platform in a New Brunswick Excella E25 (Eppendorf, CT, USA). Alternatively, single colonies from LB agar plates were inoculated in 100 µL of LB in 96-well microplates using sterile pipette tips. Each colony picked by a sterile pipette tip was subsequently mixed with the media in the target well and was grown overnight at 37°C and 400 rpm in an incubating microplate shaker.

For the microplate-based screening assay, 5 % (v/v) of cell inocula were first inoculated in 100 µL of the M9 hybrid media containing 20 g/L of glucose, 0.1 mM of isopropyl β-D-1-thiogalactopyranoside (IPTG), and 2 g/L of alcohol (i.e., ethanol, n-butanol, isobutanol, or 2-phenylethyl alcohol) in 96-well microplates with or without hexadecane overlay in a 1:1 (v/v) ratio. The microplates were then sealed with a plastic adhesive sealing film, SealPlate® (EXCEL Scientific, Inc., CA, USA), to avoid cross contamination and evaporation. Finally, the microplates were incubated at 37ºC and 400 rpm for 24 hours (h) in an incubating microplate shaker (Fisher Scientific, PA, USA).

The optical density (OD) of cell culture was measured at 600 nm using a BioTek Synergy HT microplate reader (BioTek Instruments, Inc., VT, USA). The dry cell weight (DCW) was obtained by multiplication of the optical density of culture broth with a pre-determined conversion factor, 0.385 g/L/OD. The organic layers were collected for ester measurement either by gas chromatography coupled with mass spectroscopy **(**GC/MS) or colorimetric assay.

2.4 SDS-PAGE analysis. For SDS-PAGE analysis, 1% (v/v) of stock cells were grown overnight at 37ºC and 200 rpm in 15 mL culture tubes containing 5 mL of LB media and antibiotics. Then, 4% (v/v) of the overnight cultures were transferred into 1.5 mL of LB media containing antibiotics in a 24-well microplate (cat# 353224, BD Falcon). The cultures were next grown at 37ºC and 400 rpm using an incubating microplate shaker. When the cultures reached an OD of 0.4~0.6, they were induced with 0.1 mM IPTG and sealed with a Breathe-Easy Sealing Membrane to prevent evaporation and cross contamination (cat# BEM-1, Research Products International Corp., IL, USA). After 4 h of induction, cells were collected by centrifugation and resuspended in 1X phosphate-buffered saline (PBS) buffer (pH7.4) at the final OD of 5. The cell pellets were disrupted using the B-PER complete reagent (cat# 89822,

Thermo Scientific, MA, USA). The resulting crude extracts were mixed with 6x sodium dodecyl sulfate (SDS) sample buffer and heated at 95℃ for 5 min. Finally, the protein samples were analyzed by SDS-polyacrylamide gel electrophoresis (SDS-PAGE, 14% polyacrylamide gel). Protein bands were visualized with Coomassie Brilliant Blue staining.

2.5 Gas chromatography coupled with mass spectroscopy (GC/MS). The microplates from the microbial screening of AATs were centrifuged at 4,800 x g for 5 min and the hexadecane overlays were used for quantification of esters. The samples were prepared by diluting hexadecane extracts from the cultures with hexadecane containing internal standard (isoamyl alcohol) in a 1:1 (v/v) ratio. Then, 1 μL of samples were directly injected into a gas chromatograph (GC) HP 6890 equipped with the mass selective detector (MS) HP 5973. For the GC system, helium was used as the carrier gas at a flow rate of 0.5 mL/min and the analytes were separated on a Phenomenex ZB-5 capillary column (30 m x 0.25 mm x 0.25 μm). The oven temperature was programmed with an initial temperature of 50℃ with a 1℃/min ramp to 58℃. Next a 25℃/min ramp was deployed to 235℃ and then a 50℃/min ramp was deployed to 300℃. Finally held a temperature of 300℃ for 2 minutes to elute any residual non-desired analytes. The injection was performed using the splitless mode with an initial injector temperature of 280℃. For the MS system, a selected ion monitoring (SIM) mode was deployed to detect analytes. The SIM parameters for detecting esters were as follows: i) for ethyl acetate, ions 45.00, and 61.00 detected from 4.15 to 5.70 min, ii) for isoamyl alcohol (internal standard), ions 45.00, and 88.00 detected from 5.70 to 6.60 min, iii) for isobutyl acetate, ions 61.00, and 101.00 detected from 6.60 to 7.75 min, iv) for butyl acetate, ions 61.00, and 116.00 detected from 7.75 to 13.70 min, and v) for 2-phenethyl acetate, ions 104.00, and 121.00 detected from 13.70 to 13.95 min.

2.6 Colorimetric assay for ester quantification. The colorimetric assay for ester quantification was performed in a 96-well microplate. The protocol was slightly modified from the previously reported method (Lobs et al. 2016). Specifically, in each well, 60 µL of hexadecane overlay from the culture was mixed with 20 µL of hydroxylamine stock solution and incubated in an incubating microplate shaker at room temperature for 10 minutes (min) to produce hydroxamic acid. Next, 120 µL of the ferric working solution (1/20-diluted stock ferric iron(III) solution in ethanol) was added to the reaction solution and incubated for 5 min to form an iron-hydroxamic acid complex. Finally, the absorbance was measured at 520 nm (Ab_{520}) using a BioTek Synergy HT microplate reader. Esters were quantified using a standard curve between the absorbances and known concentrations of a target ester.

2.7 *In silico* mutagenesis of AATs. The 3D structures of $ATF1_{Sc}$, acetyl-CoA, and butanol were first prepared for the model-guided protein engineering of $ATF1_{Sc}$ in MOE (Molecular Operating Environment software), as previously described (Seo et al. 2019). To perform docking simulations in MOE, the potential binding pocket of $ATF1_{Sc}$ was identified using the 'Site Finder' tool. Both of the conserved catalytic residues, H191 and D195, that are known to reside in the binding pocket of AATs (Navarro-Retamal et al. 2016), were selected. Acetyl-CoA and butanol were docked to the binding pocket of $ATF1_{Sc}$ in a sequential step. After the docking simulations, the best-scored binding poses were selected for *in silico* mutagenesis. The 'residue scan' tool of MOE was used to identify beneficial mutations for the biosynthesis of the target ester (i.e., butyl acetate) in $ATF1_{Sc}$ variants, based on their △Affinity (kcal/mol) values. Here, the △Affinity value represents the relative binding affinity between a mutant and its wild type, where a more negative value indicates a mutant with higher affinity. Details of the docking simulation and *in silico* mutagenesis analysis protocols in MOE can be found in the previous report (Lee et al. 2018).

3. RESULTS AND DISCUSSION

3.1 Establishing a microplate-based culturing technique with *in situ* fermentation and extraction of esters. To develop a high-throughput microbial screening platform for ester biosynthesis, we first examined whether the microplate-based culturing technique could be reliably used to monitor cell growth and continuously extract esters for downstream quantification. We characterized the recombinant BL21 (DE3) strains harboring 20 CAT_{Sa} F97 variants (Seo et al. 2019) in 96-well microplates for IBA production with or without solvent (hexadecane) overlay for *in situ* ester extraction (Fig. 1A). As a basis for comparison, we also performed the high cell density culturing method in shake tubes that was previously employed for AAT screening (Seo et al. 2019).

The characterization results show that IBA production in microplates followed the same trend of its production observed in high cell density cultures (Fig. 1B). Strong positive linear correlations ($R^2 \geq 0.98$) in IBA production existed between the microplate-based and high cell density culturing methods (Figs. 1C, 1D). The microplate-based culturing method could validate that the CAT_{Sa} F97W variant achieved the highest IBA production among the 20 characterized variants (Table S2). While these variants exhibited different activities toward IBA, their cell cultures exhibited similar growth (Fig. S1).

Using solvent overlays for microbial biosynthesis of esters can provide several key advantages. First, the solvent overlay enables a more reliable measurement of cell growth in microplates by avoiding medium evaporation that caused water condensation (Fig. 1E) and hence interfered with optical density measurement (Fig. S1). Growth kinetics helps evaluate the effect of expressing AATs on microbial health. Second, the solvent overlay simplifies the sample preparation step for quantification of esters and is compatible with a high-throughput workflow, where esters in the solvent layer can be extracted for downstream measurement by either a GC/MS method or a colorimetric assay (Layton and Trinh 2014; Layton and Trinh

2016a; Layton and Trinh 2016b; Lobs et al. 2016; Rodriguez et al. 2014). Third, the solvent overlay helps alleviate the product toxicity during fermentation (Brennan et al. 2012) because esters are known to be inhibitory to microbial health (Wilbanks and Trinh 2017).

Taken altogether, the microplate-based culturing method with solvent overlays is reliable and suitable for a rapid, high-throughput *in vivo* screening platform for microbial ester production.

3.2 Revealing the influential role of CAT_{Sa} F97 residue by profiling alcohol preference of a library of F97 mutants with the microplate-based culturing method. Our previous study discovered that the CAT_{Sa} F97W mutant improved its catalytic efficiency towards isobutanol by ~2-fold (Seo et al. 2019). We hypothesized that the F97 residue might have an important role in determining the alcohol substrate preference. Using the established microplate-based culturing method, we evaluated whether it could be used for rapid profiling of the alcohol substrate preference of CAT_{Sa} F97 variants. We characterized the recombinant *E. coli* strains carrying 20 CAT_{Sa} F97 variants with exogenous supplementation of alcohols in the media including linear, short-chain alcohols (ethanol, butanol), a branched-chain alcohol (isobutanol), and an aromatic alcohol (2-phenylethyl alcohol) in microplates with hexadecane overlay.

The characterization results showed that mutations in the F97 residue changed the ester production profiles (Fig. 2A, Table S3), suggesting that F97 plays an important role in determining the alcohol substrate preference of CAT_{Sa}. All the CAT_{Sa} variants exhibited poor activities toward ethanol (Table S3). Among the four target acetate esters investigated, F97H produced 2-phenylethyl acetate (PEA) at the highest level of 194.63 mg/L followed by F97H (182.30 mg/L) and the wildtype F97 (149.41 mg/L) (Fig. 2A, Table S3). As compared to the wildtype, IBA production by F97W (91.22 mg/L) showed the highest improvement (~6.39-fold) (Fig. 2A, Table S3), which was relatively consistent with the prior *in vitro* study showing

that F97W variant achieved ~2-fold increase in the catalytic efficiency towards isobutanol (Seo et al. 2019). Remarkably, F97T showed BA production (12.42 mg/L) with high specificity, demonstrating the feasibility of production of designer esters using re-programmed CATs (Fig. 2A, Table S3). Different from F97W, F97C exhibited the highest n-butyl acetate (BA) production (18.26 mg/L) (Fig. 2A, Table S3). Examining the protein structure of CAT_{Sa} can provide some insights its alcohol substrate preference (Fig. 2B). As shown, the binding pockets of CATs are formed at the subunit interfaces (Day and Shaw 1992) and the F97 residue located on the opposite subunit of the catalytic residues, H189 and D193. One possible explanation on how only one residue replacement influences the substrate preference of CAT_{Sa} is that the mutation in the F97 residue might dramatically change the size and/or shape of the binding pocket and hence alternate the interactions among subunits of CAT_{Sa}.

Taken altogether, the microplate-based culturing method coupled with GC/MS can be employed for rapid profiling of substrate preferences of AATs. The method revealed the important role of the F97 residue in determining the alcohol substrate preference of CAT_{Sa}.

3.3 Developing a high-throughput microbial screening platform for ester biosynthesis by integration of the microplate-based culturing method and a colorimetric assay. High-throughput screening of ester biosynthesis has been limited by the use of GC/MS. Since the reactions of esters with hydroxylamine generate hydroxamic acids that form purple complexes with ferric ion, esters can be determined colorimetrically by measuring absorbance at 520 nm (Fig. 3A, 3B) (Hill 1946; Lobs et al. 2016; Stern and Shapiro 1953; Wofford et al. 1986). This colorimetric assay has recently been adapted for high-throughput screening of ethyl acetate (EA) production from C5, C6, and C12 carbon sources in *Kluyveromyces marxianus* (Lobs et al. 2016) where cell culture samples were first collected followed by ester extraction with hexane. This protocol is useful but might not be compatible with the microplate-based culturing

293 method in our study because hexane is toxic and hence cannot be used for *in situ* fermentation
294 and extraction, unlike hexadecane. Here, we tested whether the colorimetric assay can be
295 modified and coupled with the microplate-based culturing method to facilitate a high-
296 throughput microbial screening of AATs for ester biosynthesis.

297 To compare ester quantification by the colorimetric assay and GC/MS method, we
298 analyzed IBA production by the *E. coli* BL21 (DE3) strains harboring the 20 F97 variants as
299 demonstrated for microplate-based culturing method. We started by developing a standard
300 curve to estimate IBA production by the colorimetric assay. Using pure IBA in hexadecane, an
301 almost perfect linear correlation (R^2=0.999) was established between absorbance at 520 nm
302 and IBA concentration within 0-200 mg/L (Fig. 3C). When using esters in hexadecane from
303 the cell culture samples for the colorimetric assay, we found that the colorimetric assay could
304 determine the IBA concentrations consistently with the GC/MS method (Fig. 3D).

305 Critical to the high-throughput microbial screening method to estimate the target esters
306 from the culture samples is to have an appropriate control for the baseline adjustment in the
307 colorimetric assay. In our study, we found that the colorimetric method could overestimate the
308 IBA production as compared to the GC/MS method (Fig. S2B, Table S4). Since the *E. coli* host
309 produced ethanol endogenously, EA was produced as an inevitable by-product (Fig. S2A),
310 causing the observed IBA overestimation. To avoid this problem, we used ΔAb_{520} for
311 estimating IBA production where $\Delta Ab_{520} = Ab_{520,\ AAT^+,\ ROH^+} - Ab_{520,\ AAT^+,\ ROH^-}$ is the absorbance
312 difference between culture samples with and without the target alcohol (ROH) availability. The
313 target alcohol can be supplemented externally or produced by the cells. One other strategy that
314 might help avoid the target ester (e.g., IBA) overestimation problem by the colorimetric assay
315 is to use a host strain void of the endogenous pathways causing the biosynthesis of the
316 unwanted alcohol byproduct (e.g., ethanol).

317 It is important to note that during our protocol development, we observed that the
318 perturbed, emulsified layer of an immiscible hexadecane-ethanol mixture interfered with the
319 measured absorbance and generated irreproducible data. Note that ethanol is originated from
320 the ferric solution used in the colorimetric assay. This problem did not occur in the previous
321 study (Lobs et al. 2016) likely because hexane used for ester extraction is miscible in ethanol.
322 To address this problem, we used a centrifugation step to create the immiscible hexadecane-
323 ethanol mixture with the transparent organic phase and strong purple aqueous phase (Fig. 3B).
324 Overall, the microplate-based culturing method coupled with a colorimetric assay is
325 suitable for high-throughput microbial screening of AATs for ester biosynthesis.
326
327 **3.4 Combining the model-guided protein engineering and high-throughput microbial**
328 **screening platform to rapidly identify ATF1$_{Sc}$ variants for improved BA production**
329 With the established high-throughput microbial screening platform, we applied it to rapidly
330 identify the engineered ATF1$_{Sc}$ mutants for enhanced BA production (Fig. 4A). We started by
331 generating a library of potential ATF1$_{Sc}$ candidates for improved BA production *in silico* for
332 high-throughput microbial screening. To do this, we first created a 3-D structure of ATF1$_{Sc}$
333 using the homology model of 15-O-acetyltransferase (PDB:3FP0) best predicted by SWISS-
334 MODEL (Waterhouse et al. 2018). We next identified the binding pocket of ATF1$_{Sc}$ for
335 docking simulations of the BA co-substrates, including acetyl-CoA and butanol. Based on the
336 homology model, the binding pocket of ATF1$_{Sc}$ consists of 24 residues including V32, Y36,
337 H191, D195, G196, R197, T316, I347, P348, A349, D350, R352, N370, V371, I374, F376,
338 Y399, I403, L407, K426, L448, S449, N450, V451, F471, and Q473, where H191 and D195
339 are the catalytic residues (Fig. S3A). By performing docking simulations, we generated the
340 acetyl-CoA-butanol-ATF1$_{Sc}$ complex and identified the residues interacting with butanol
341 including V32, Y36, D195, P348, V371, L447, S449, Q473, Q475, and S483 (Fig. S3B).

Finally, we performed the residue scan against these 10 residues to select the top 12 promising candidates including P348W, P348R, P348M, P348H, P348K, P348N, P348I, P348S, P348D, P348C, P348A, and P348Q for experimental characterization (Fig. 4B).

To perform the high-throughput microbial screening of the top 12 engineered $ATF1_{Sc}$ candidates for improved BA production, we used TCS083 △*fadE* (DE3) (Layton and Trinh 2014) as a host strain. Like the colorimetric assay developed for IBA measurement, the standard curve for BA measurement showed a strong linear correlation (R^2=0.999) between the 520 nm absorbance and the standard BA concentrations in the range of 0-200 mg/L (Fig. 4C). Our screening results shows that the P348M, P348A, or P348S mutation in $ATF1_{Sc}$ improved BA production by 3.34, 2.90, or 2.88-fold, respectively (Fig. 4D). To confirm this result, we compared the BA titers measured by the colorimetric assay with those by GC/MS. Remarkably, we could observe almost identical BA titers between the two methods (Table S5) with a strong linear correlation (R^2=0.973) (Fig. 4E). This result demonstrates the high-throughput microbial screening platform is suitable for rapidly identifying AATs for designer ester biosynthesis. Interestingly, like the F97 residue in CAT_{Sa} (Fig. 2B), the P348 residue in $ATF1_{Sa}$ is also located on the opposite side of the catalytic residues including H191 and D195 (Fig. 4F) and interacts with an alcohol substrate, which might determine the alcohol substrate preference.

Overall, we rationally engineered $ATF1_{Sc}$ for improved BA production through a model-guided rational protein engineering and rapidly identified the beneficial $ATF1_{Sc}$ variants using the established high-throughput microbial screening platform.

4. CONCLUSION

We developed a high-throughput microbial screening platform to probe specificities of AATs/CATs for designer ester biosynthesis. This platform integrated the microplate culturing method with a modified colorimetric assay previously established, which provides useful

information about AAT expression and activity, microbial health, and ester production. For the microplate-based culturing protocol, the use of solvent overlays is critical to minimize medium evaporation, generate reproducible growth measurement, and eliminate the ester extraction step. For colorimetric assay, the addition of a centrifugation step is crucial to avoid the interference of ethanol-hexadecane immiscible layer that causes irreproducible measurement. The high-throughput microbial screening platform not only confirmed CAT_{Sa} F97W with enhanced isobutyl acetate synthesis but also identified the three $ATF1_{Sc}$ (P348M, P348A, and P348S) variants generated by model-guided rational protein engineering for enhanced butyl acetate production. Overall, this study presents a high-throughput microbial screening platform for rapid profiling of the alcohol substrate preference of AATs for production of designer esters. We believe that this platform is scalable and compatible with automated microplate handling systems to increase its screening capacity.

ACKNOWLEDGEMENTS

This research was financially supported in part by the NSF CAREER award (NSF#1553250), the DOE BER Genomic Science Program (DE-SC0019412), and the DOE subcontract grant (DE-AC05-000R22725) by the Center of Bioenergy Innovation, the U.S. Department of Energy Bioenergy Research Center funded by the Office of Biological and Environmental Research in the DOE Office of Science, and the U.S. Department of Energy Joint Genome Institute. The authors would like to thank the Center of Environmental Biotechnology at UTK for using the GC/MS instrument.

REFERENCES

Aharoni A, Keizer LCP, Bouwmeester HJ, Sun ZK, Alvarez-Huerta M, Verhoeven HA, Blaas J, van Houwelingen AMML, De Vos RCH, van der Voet H and others. 2000. Identification of the SAAT gene involved in strawberry flavor biogenesis by use of DNA microarrays. Plant Cell 12(5):647-661.

Balbontin C, Gaete-Eastman C, Fuentes L, Figueroa CR, Herrera R, Manriquez D, Latche A, Pech JC, Moya-Leon MA. 2010. VpAAT1, a Gene Encoding an Alcohol Acyltransferase, Is Involved in Ester Biosynthesis during Ripening of Mountain Papaya Fruit. Journal of Agricultural and Food Chemistry 58(8):5114-5121.

Beekwilder J, Alvarez-Huerta M, Neef E, Verstappen FWA, Bouwmeester HJ, Aharoni A. 2004. Functional characterization of enzymes forming volatile esters from strawberry and banana. Plant Physiology 135(4):1865-1878.

Brennan TC, Turner CD, Kromer JO, Nielsen LK. 2012. Alleviating monoterpene toxicity using a two-phase extractive fermentation for the bioproduction of jet fuel mixtures in Saccharomyces cerevisiae. Biotechnol Bioeng 109(10):2513-22.

Chacon MG, Kendrick EG, Leak DJ. 2019. Engineering Escherichia coli for the production of butyl octanoate from endogenous octanoyl-CoA. Peerj 7.

Cumplido-Laso G, Medina-Puche L, Moyano E, Hoffmann T, Sinz Q, Ring L, Studart-Wittkowski C, Caballero JL, Schwab W, Munoz-Blanco J and others. 2012. The fruit ripening-related gene FaAAT2 encodes an acyl transferase involved in strawberry aroma biogenesis. Journal of Experimental Botany 63(11):4275-4290.

Day PJ, Shaw WV. 1992. Acetyl coenzyme A binding by chloramphenicol acetyltransferase. Hydrophobic determinants of recognition and catalysis. J Biol Chem 267(8):5122-7.

El-Sharkawy I, Manriquez D, Flores FB, Regad F, Bouzayen M, Latche A, Pech JC. 2005. Functional characterization of a melon alcohol acyl-transferase gene family involved in the

414 biosynthesis of ester volatiles. Identification of the crucial role of a threonine residue for
415 enzyme activity*. Plant Mol Biol 59(2):345-62.
416 Gibson DG, Young L, Chuang RY, Venter JC, Hutchison CA, Smith HO. 2009. Enzymatic
417 assembly of DNA molecules up to several hundred kilobases. Nature Methods 6(5):343-U41.
418 Gonzalez M, Gaete-Eastman C, Valdenegro M, Figueroa CR, Fuentes L, Herrera R, Moya-
419 Leon MA. 2009. Aroma Development during Ripening of Fragaria chiloensis Fruit and
420 Participation of an Alcohol Acyltransferase (FcAAT1) Gene. Journal of Agricultural and Food
421 Chemistry 57(19):9123-9132.
422 Gonzalez-Aguero M, Troncoso S, Gudenschwager O, Campos-Vargas R, Moya-Leon MA,
423 Defilippi BG. 2009. Differential expression levels of aroma-related genes during ripening of
424 apricot (Prunus armeniaca L.). Plant Physiology and Biochemistry 47(5):435-440.
425 Hill UT. 1946. Colorimetric Determination of Fatty Acids and Esters. Industrial and
426 Engineering Chemistry-Analytical Edition 18(5):317-319.
427 Knight MJ, Bull ID, Curnow P. 2014. The yeast enzyme Eht1 is an octanoyl-CoA:ethanol
428 acyltransferase that also functions as a thioesterase. Yeast 31(12):463-74.
429 Kruis AJ, Levisson M, Mars AE, van der Ploeg M, Daza FG, Ellena V, Kengen SWM, van der
430 Oost J, Weusthuis RA. 2017. Ethyl acetate production by the elusive alcohol acetyltransferase
431 from yeast. Metabolic Engineering 41:92-101.
432 Layton DS, Trinh CT. 2014. Engineering modular ester fermentative pathways in Escherichia
433 coli. Metabolic Engineering 26:77-88.
434 Layton DS, Trinh CT. 2016a. Expanding the modular ester fermentative pathways for
435 combinatorial biosynthesis of esters from volatile organic acids. Biotechnol Bioeng
436 113(8):1764-76.
437 Layton DS, Trinh CT. 2016b. Microbial synthesis of a branched-chain ester platform from
438 organic waste carboxylates. Metab Eng Commun 3:245-251.

439 Layton DS, Trinh, C.T. 2014. Engineering Modular Ester Fermentative Pathways in
440 *Escherichia coli*. Metab Eng. 26:77-88.
441 Lee J, Trinh CT. 2018. De novo Microbial Biosynthesis of a Lactate Ester Platform.
442 bioRxiv:498576.
443 Lee JW, Niraula NP, Trinh CT. 2018. Harnessing a P450 fatty acid decarboxylase from
444 Macrococcus caseolyticus for microbial biosynthesis of odd chain terminal alkenes. Metab
445 Eng Commun 7:e00076.
446 Lee JW, Trinh CT. 2019. Microbial biosynthesis of lactate esters. Biotechnology for Biofuels
447 12(1).
448 Lee JW, Trinh CT. 2020. Towards renewable flavors, fragrances, and beyond. Current Opinion
449 in Biotechnology 61:168-180.
450 Li DP, Xu YF, Xu GM, Gu LK, Li DQ, Shu HR. 2006. Molecular cloning and expression of a
451 gene encoding alcohol acyltransferase (MdAAT2) from apple.(cv. Golden Delicious).
452 Phytochemistry 67(7):658-667.
453 Lin JL, Zhu J, Wheeldon I. 2016. Rapid ester biosynthesis screening reveals a high activity
454 alcohol-O-acyltransferase (AATase) from tomato fruit. Biotechnology Journal 11(5):700-707.
455 Lobs AK, Lin JL, Cook M, Wheeldon I. 2016. High throughput, colorimetric screening of
456 microbial ester biosynthesis reveals high ethyl acetate production from Kluyveromyces
457 marxianus on C5, C6, and C12 carbon sources. Biotechnol J 11(10):1274-1281.
458 Lucchetta L, Manriquez D, El-Sharkawy I, Flores FB, Sanchez-Bel P, Zouine M, Ginies C,
459 Bouzayen M, Rombaldi C, Pech JC and others. 2007. Biochemical and catalytic properties of
460 three recombinant alcohol acyltransferases of melon. Sulfur-containing ester formation,
461 regulatory role of CoA-SH in activity, and sequence elements conferring substrate preference.
462 Journal of Agricultural and Food Chemistry 55(13):5213-5220.

463 Navarro-Retamal C, Gaete-Eastman C, Herrera R, Caballero J, Alzate-Morales JH. 2016.
464 Structural and Affinity Determinants in the Interaction between Alcohol Acyltransferase from
465 F. x ananassa and Several Alcohol Substrates: A Computational Study. Plos One 11(4).
466 Rodriguez GM, Tashiro Y, Atsumi S. 2014. Expanding ester biosynthesis in Escherichia coli.
467 Nature Chemical Biology 10(4):259-+.
468 Seo H, Lee J-W, Giannone RJ, Dunlap NJ, Trinh CT. 2020. Repurposing chloramphenicol
469 acetyltransferase for a robust and efficient designer ester biosynthesis platform. bioRxiv.
470 Seo H, Lee JW, Garcia S, Trinh CT. 2019. Single mutation at a highly conserved region of
471 chloramphenicol acetyltransferase enables isobutyl acetate production directly from cellulose
472 by Clostridium thermocellum at elevated temperatures. Biotechnology for Biofuels 12(1).
473 Souleyre EJF, Chagne D, Chen XY, Tomes S, Turner RM, Wang MY, Maddumage R, Hunt
474 MB, Winz RA, Wiedow C and others. 2014. The AAT1 locus is critical for the biosynthesis
475 of esters contributing to "ripe apple' flavour in "Royal Gala' and "Granny Smith' apples. Plant
476 Journal 78(6):903-915.
477 Souleyre EJF, Greenwood DR, Friel EN, Karunairetnam S, Newcomb RD. 2005. An alcohol
478 acyl transferase from apple (cv. Royal Gala), MpAAT1, produces esters involved in apple fruit
479 flavor. Febs Journal 272(12):3132-3144.
480 Stern I, Shapiro B. 1953. A Rapid and Simple Method for the Determination of Esterified Fatty
481 Acids and for Total Fatty Acids in Blood. Journal of Clinical Pathology 6(2):158-160.
482 Tai Y-S, Xiong M, Zhang K. 2015a. Engineered biosynthesis of medium-chain esters in
483 Escherichia coli. Metabolic Engineering 27:20-28.
484 Tai YS, Xiong MY, Zhang KC. 2015b. Engineered biosynthesis of medium-chain esters in
485 Escherichia coli. Metabolic Engineering 27:20-28.
486 Verstrepen KJ, Van Laere SD, Vanderhaegen BM, Derdelinckx G, Dufour JP, Pretorius IS,
487 Winderickx J, Thevelein JM, Delvaux FR. 2003. Expression levels of the yeast alcohol

488 acetyltransferase genes ATF1, Lg-ATF1, and ATF2 control the formation of a broad range of
489 volatile esters. Appl Environ Microbiol 69(9):5228-37.
490 Waterhouse A, Bertoni M, Bienert S, Studer G, Tauriello G, Gumienny R, Heer FT, de Beer
491 TAP, Rempfer C, Bordoli L and others. 2018. SWISS-MODEL: homology modelling of
492 protein structures and complexes. Nucleic Acids Research 46(W1):W296-W303.
493 Wilbanks B, Trinh CT. 2017. Comprehensive characterization of toxicity of fermentative
494 metabolites on microbial growth. Biotechnology for Biofuels 10(1):262.
495 Wofford NQ, Beaty PS, Mcinerney MJ. 1986. Preparation of Cell-Free-Extracts and the
496 Enzymes Involved in Fatty-Acid Metabolism in Syntrophomonas-Wolfei. Journal of
497 Bacteriology 167(1):179-185.
498 Zheng L, Baumann U, Reymond JL. 2004. An efficient one-step site-directed and site-
499 saturation mutagenesis protocol. Nucleic Acids Res 32(14):e115.
500
501

502 **Table 1:** The list of plasmids and strains used in this study.

Name	Description	Source
Strains		
E. coil TOP10	F⁻ *mcr*A Δ(*mrr-hsd*RMS-*mcr*BC) φ80*lac*ZΔM15 Δ*lac*X74 *rec*A1 *ara*D139 Δ(*ara-leu*)7697 *gal*U *gal*K λ⁻ *rps*L(Str^R) *end*A1 *nup*G	Invitrogen
BL21 (DE3)	F⁻ *omp*T *hsd*S$_B$ (r_B^- m_B^-) *gal dcm* (DE3)	Invitrogen
EcDL002	TCS083 Δ*fadE* (DE3)	(Layton and Trinh 2014)
Plasmids		
pCAT$_{Sa}$	pETDuet-1 carrying CAT$_{Sa}$; Amp^R	(Seo et al. 2019)
pCAT$_{Sa}$ F97R	pETDuet-1 carrying CAT$_{Sa}$ F97R; Amp^R	(Seo et al. 2019)
pCAT$_{Sa}$ F97H	pETDuet-1 carrying CAT$_{Sa}$ F97H; Amp^R	(Seo et al. 2019)
pCAT$_{Sa}$ F97K	pETDuet-1 carrying CAT$_{Sa}$ F97K; Amp^R	(Seo et al. 2019)
pCAT$_{Sa}$ F97D	pETDuet-1 carrying CAT$_{Sa}$ F97D; Amp^R	(Seo et al. 2019)
pCAT$_{Sa}$ F97E	pETDuet-1 carrying CAT$_{Sa}$ F97E; Amp^R	(Seo et al. 2019)
pCAT$_{Sa}$ F97S	pETDuet-1 carrying CAT$_{Sa}$ F97S; Amp^R	(Seo et al. 2019)
pCAT$_{Sa}$ F97T	pETDuet-1 carrying CAT$_{Sa}$ F97T; Amp^R	(Seo et al. 2019)
pCAT$_{Sa}$ F97N	pETDuet-1 carrying CAT$_{Sa}$ F97N; Amp^R	(Seo et al. 2019)
pCAT$_{Sa}$ F97Q	pETDuet-1 carrying CAT$_{Sa}$ F97Q; Amp^R	(Seo et al. 2019)
pCAT$_{Sa}$ F97C	pETDuet-1 carrying CAT$_{Sa}$ F97C; Amp^R	(Seo et al. 2019)
pCAT$_{Sa}$ F97G	pETDuet-1 carrying CAT$_{Sa}$ F97G; Amp^R	(Seo et al. 2019)
pCAT$_{Sa}$ F97Y	pETDuet-1 carrying CAT$_{Sa}$ F97Y; Amp^R	(Seo et al. 2019)
pCAT$_{Sa}$ F97P	pETDuet-1 carrying CAT$_{Sa}$ F97P; Amp^R	(Seo et al. 2019)
pCAT$_{Sa}$ F97A	pETDuet-1 carrying CAT$_{Sa}$ F97A; Amp^R	(Seo et al. 2019)
pCAT$_{Sa}$ F97V	pETDuet-1 carrying CAT$_{Sa}$ F97V; Amp^R	(Seo et al. 2019)
pCAT$_{Sa}$ F97I	pETDuet-1 carrying CAT$_{Sa}$ F97I; Amp^R	(Seo et al. 2019)
pCAT$_{Sa}$ F97L	pETDuet-1 carrying CAT$_{Sa}$ F97L; Amp^R	(Seo et al. 2019)
pCAT$_{Sa}$ F97M	pETDuet-1 carrying CAT$_{Sa}$ F97M; Amp^R	(Seo et al. 2019)
pCAT$_{Sa}$ F97W	pETDuet-1 carrying CAT$_{Sa}$ F97W; Amp^R	(Seo et al. 2019)
pDL004	pETite carrying ATF1$_{Sc}$; Kan^R	(Layton and Trinh 2016a)
pATF1$_{Sc}$	pET29 carrying ATF1$_{Sc}$; Kan^R	This study
pATF1$_{Sc}$ P348W	pET29 carrying ATF1$_{Sc}$ P348W; Kan^R	This study
pATF1$_{Sc}$ P348R	pET29 carrying ATF1$_{Sc}$ P348R; Kan^R	This study
pATF1$_{Sc}$ P348M	pET29 carrying ATF1$_{Sc}$ P348M; Kan^R	This study
pATF1$_{Sc}$ P348H	pET29 carrying ATF1$_{Sc}$ P348H; Kan^R	This study
pATF1$_{Sc}$ P348K	pET29 carrying ATF1$_{Sc}$ P348K; Kan^R	This study
pATF1$_{Sc}$ P348N	pET29 carrying ATF1$_{Sc}$ P348N; Kan^R	This study
pATF1$_{Sc}$ P348I	pET29 carrying ATF1$_{Sc}$ P348I; Kan^R	This study
pATF1$_{Sc}$ P348S	pET29 carrying ATF1$_{Sc}$ P348S; Kan^R	This study
pATF1$_{Sc}$ P348D	pET29 carrying ATF1$_{Sc}$ P348D; Kan^R	This study
pATF1$_{Sc}$ P348C	pET29 carrying ATF1$_{Sc}$ P348C; Kan^R	This study
pATF1$_{Sc}$ P348A	pET29 carrying ATF1$_{Sc}$ P348A; Kan^R	This study
pATF1$_{Sc}$ P348Q	pET29 carrying ATF1$_{Sc}$ P348Q; Kan^R	This study

503

504

FIGURE LEGENDS

Figure 1. A microplate-based culturing method for microbial biosynthesis of esters with *in situ* product extraction. **(A)** Workflow of the microplate-based culturing method. (**B**) Comparison of IBA production among three different culturing methods by the recombinant BL21 (DE3) strains carrying the 20 CAT_{Sa} F97 variants after 24 h. (**C-D**) Comparison of **(C)** IBA titer and **(D)** specific productivity among three different culturing methods. The error bars represent standard deviation of four biological replicates (*n*=4). (**E**) Effect of solvent overlay on growth kinetics measurement in the microplate-based culturing method.

Figure 2. Rapid profiling of the alcohol substrate preference of CAT_{Sa} F97 variants. (**A**) Relative fold change in ester production to wild type. (**B**) The 3D structure of homology model of CAT_{Sa} and the reaction mechanism. F97 residue (in green); catalytic residues H189 and D193 (in cyan); binding pockets (in grey clouds). Note: ethyl acetate production was not shown here due to low or no detectable amounts (Table S3).

Figure 3. Development of the high-throughput microbial screening platform. (**A**) Chemical reactions involved in the colorimetric assay for ester quantification. (**B**) Demonstration of the colorimetric assay in a microplate conducted for hexadecane overlay samples and a series of IBA standards at different concentrations. (**C**) The IBA standard curve. (**D**) Comparison of the IBA titers measured by the high-throughput microbial screening and GC/MS methods. The error bars represent standard deviation of three biological replicates (*n*=3).

Figure 4. Rapid identification of the beneficial $ATF1_{Sc}$ variants for improved butyl acetate (BA) production. (**A**) A schematic workflow of the high-throughput microbial screening platform used to identify $ATF1_{Sc}$ from a library of variants generated by the model-aided protein design.

530 (**B**) Residue scan results of the residues interacting with butanol in the acetyl-CoA-butanol-
531 ATF1$_{Sc}$ complex. The orange bars represent the selected top 12 candidates for further studies.
532 (**C**) The BA standard curve used for the quantification of BA in the colorimetric assay. (**D**)
533 Screening results of the selected top 12 candidates. The error bars represent standard deviation
534 of four biological replicates (*n*=4). (**E**) Correlation of the measured BA titer between the
535 colorimetric assay and GC/MS methods. (**F**) The location of P348 residue in ATF1$_{Sc}$. A yellow
536 cloud represents a binding pocket of ATF1$_{Sc}$.
537
538

Figure 1

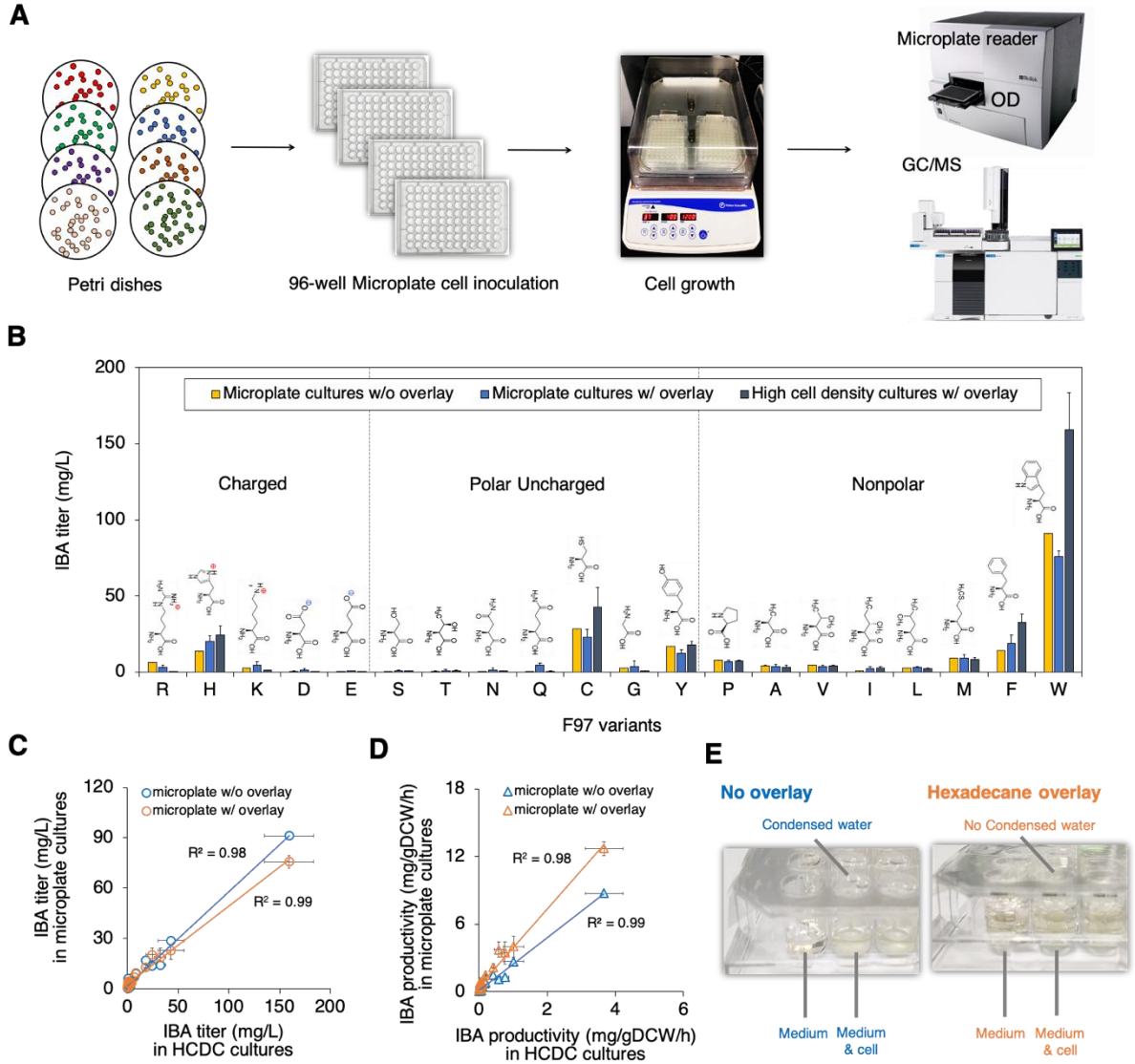

544 **Figure 2**

545

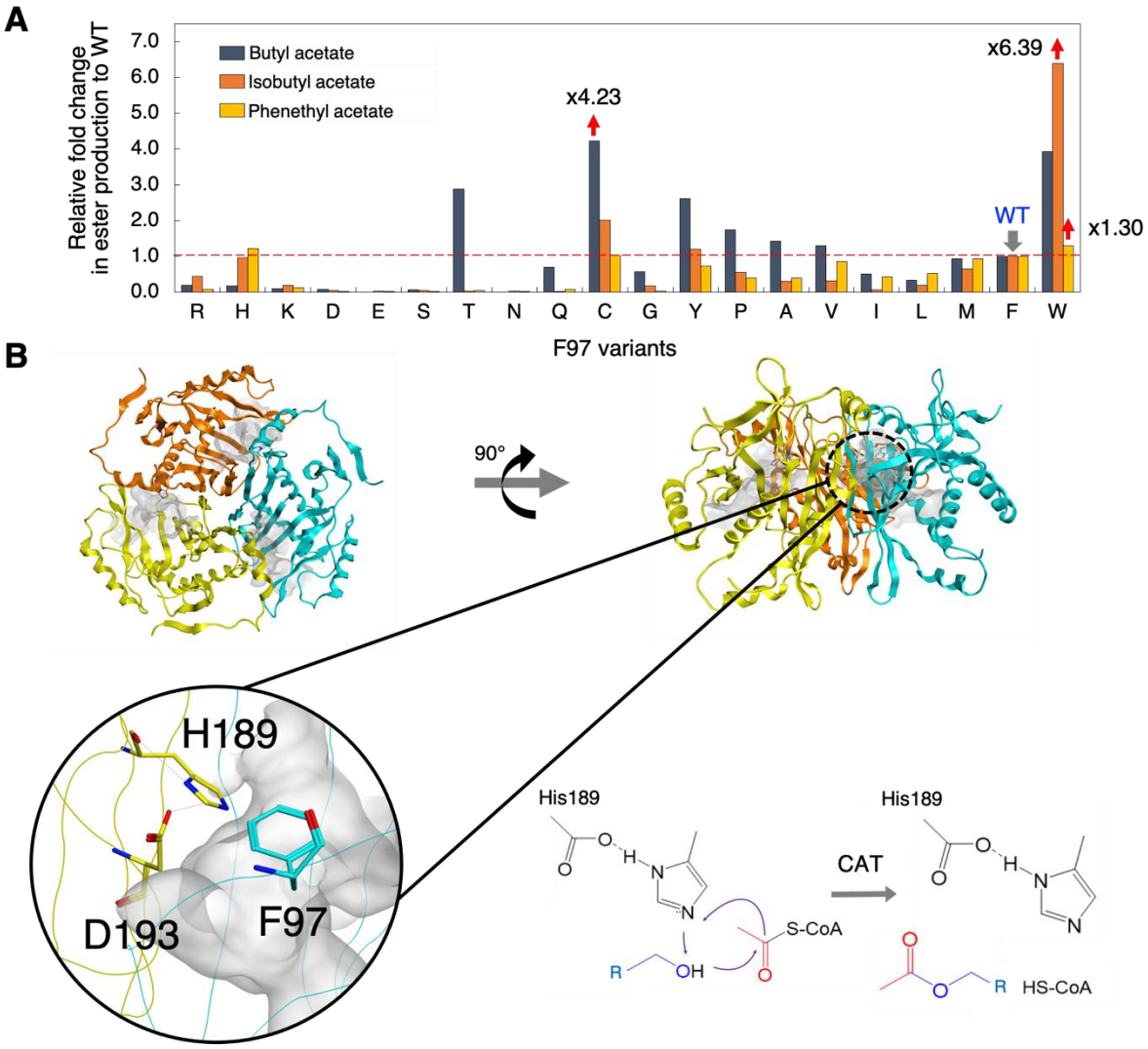

546

547

548 **Figure 3**

549

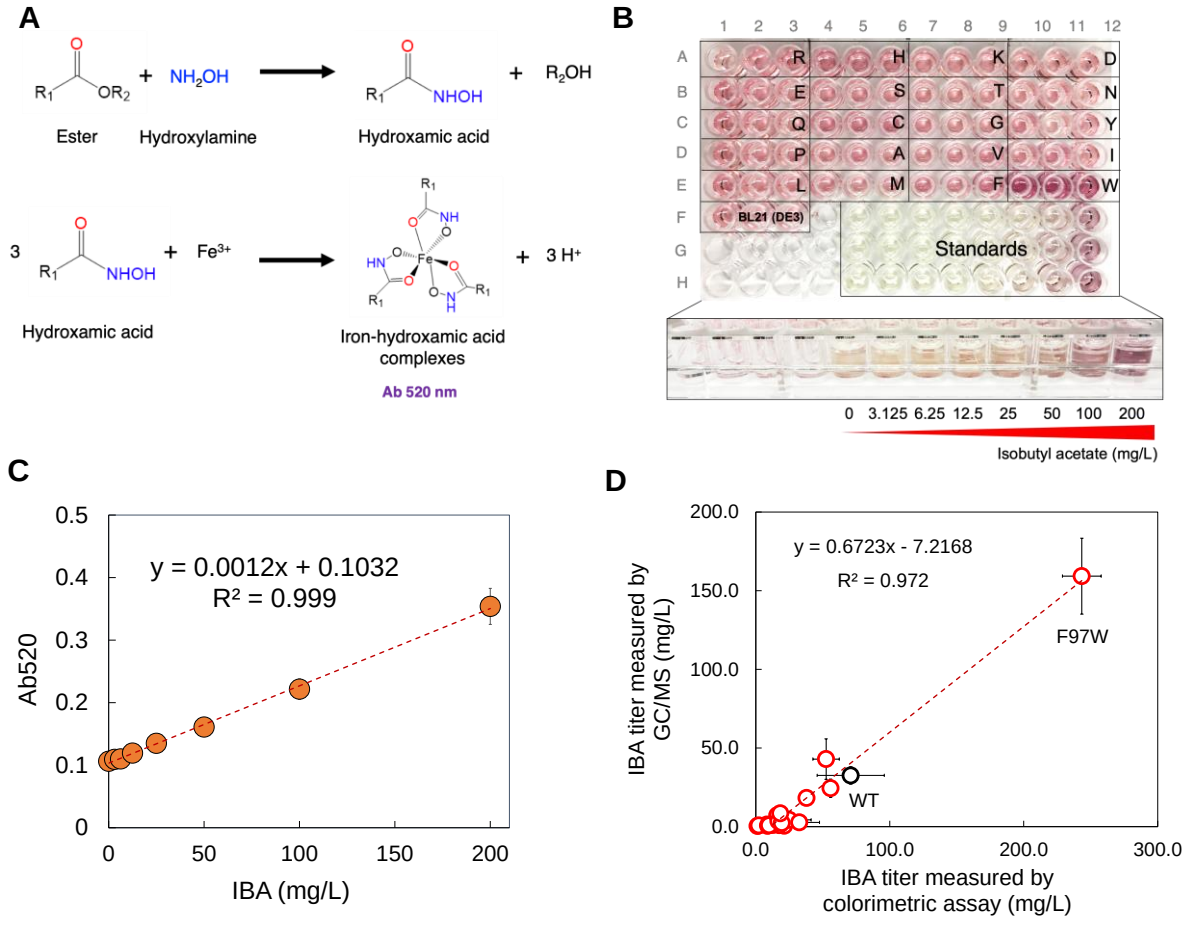

550

551

552

553 **Figure 4**

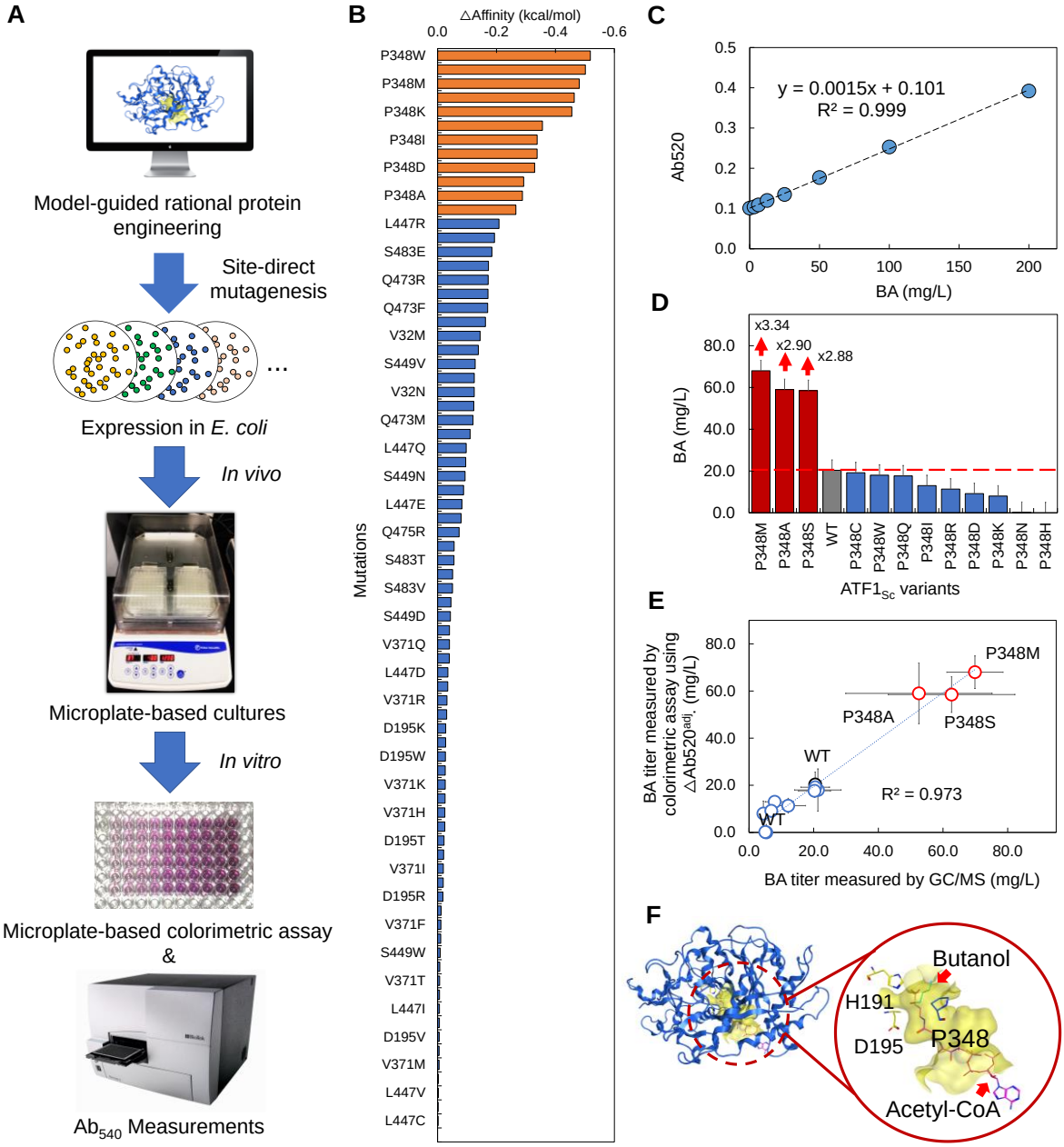

554

555

556